Chemical Science

EDGE ARTICLE

View Article Online
View Journal | View Issue

Cite this: *Chem. Sci.*, 2016, **7**, 1109

CeO_2 nanowires self-inserted into porous Co_3O_4 frameworks as high-performance "noble metal free" hetero-catalysts†

Xiao Wang, Shuna Zhao, Yibo Zhang, Zhuo Wang, Jing Feng, Shuyan Song* and Hongjie Zhang*

Received 11th September 2015
Accepted 28th October 2015

DOI: 10.1039/c5sc03430b

www.rsc.org/chemicalscience

Recently, mixed metal oxides have attracted tremendous interest because of their great importance for fundamental studies and practical applications in the catalytic field to replace expensive noble metals. Herein, we report the designed synthesis of novel CeO_2–Co_3O_4 mixed metal oxides with complex nanostructures using uniform short CeO_2 nanowires self-inserted into ZIF-67 nanocrystals as precursors followed by a thermal annealing treatment. Interestingly, such a synthetic strategy can be easily extended to fabricate other CeO_2 nanowires inserted into metal oxide nanoframeworks such as $NiCo_2O_4$ and $ZnCo_2O_4$. Choosing the NO reduction reaction by CO as the catalytic model, the as-obtained CeO_2–Co_3O_4 hybrids exhibited enhanced catalytic performance, which could be attributed to the strong two-phase interaction between each component.

Introduction

In hetero-catalytic reactions, ceria (CeO_2)-based nanomaterials have been used as efficient catalysts due to their high oxygen storage capability, good redox properties, and low cost as well as being green materials.[1–4] Many efforts have been made to develop CeO_2-based noble metal hybrid nanocatalysts with remarkably activity and long-term stability for three-way catalytic reactions (TWCs) to eliminate toxic automobile exhaust fumes, low-temperature water–gas shift (WGS) reactions, oxygen sensors, oxygen permeation membrane systems and fuel cells, but they suffer from such drawbacks as high cost, limited availability and relatively low selectivity at high temperatures which limit their widespread application.[5–8] The development of CeO_2-based "noble metal-free" nanocatalysts is an urgent and important problem to be solved. A widely accepted viewpoint for the successful fabrication of "noble metal-free" catalysts is to hybridize together multiple components with a strong synergistic effect.[9–12] Otherwise, it is found that the as-formed two-phase interface area can strongly affect the catalytic process, such as the adsorption–desorption rate of the substrate molecules and the stability of the intermediate state.[13–18] In recent years, more attention has been focused on the development of a large number of CeO_2-based mixed metal oxides including CeO_2–CuO,[9–11] CeO_2–Cu_2O,[12,13] CeO_2–Co_3O_4,[14,15] CeO_2–ZnO,[16] CeO_2–NiO[18] *et al.*

Generally speaking, the hybrid nanostructure and morphology of the building blocks play important roles in determining the catalytic performance, which can cause great differences in the two-phase interface state and the interface area as well as the anti-sintering ability. In particular, one-dimensional and porous nanomaterials have received continuous attentions owing to their combination of carrier directed motion, anisotropism, high surface area, low density, and high loading capacity.[19–23] The presence of nanoscale porous interiors with a functional one-dimensional component endows them with technological significance in catalytic applications. However, the synthesis of CeO_2-based mixed metal oxides with necessary structure is still problematic because of the difficulties in simultaneously manipulating different materials with distinct physical and chemical properties during the conventional synthesis processes. Therefore, it is still a great challenge to create novel and complex CeO_2-based metal oxides.

It is noticed that the thermolysis of metal–organic frameworks (MOFs) route under certain atmosphere is an efficient way to produce highly porous transition metal oxide nanostructures.[24–28] The sacrificial MOF templates determine directly the shape and size of the resultant porous structures by engaging themselves as consumable reactants for shell construction.[29,30] In addition, the growth process of the MOF precursor is easily controlled to obtain MOF nanocrystals with desired morphology, size and composition on a variety of substrates. Inspired by recently achieved progress, herein we demonstrate a novel approach for the effective synthesis of

State Key Laboratory of Rare Earth Resource Utilization, Changchun Institute of Applied Chemistry, Chinese Academy of Sciences, Changchun 130022, P. R. China. E-mail: songsy@ciac.ac.cn; hongjie@ciac.ac.cn

† Electronic supplementary information (ESI) available: XRD data of pure CeO_2 nanowires; TG curve of CeO_2–ZIF-67-2 precursor; XPS and N_2 adsorption–desorption isotherm data of CeO_2–Co_3O_4-2 sample and ICP data. See DOI: 10.1039/c5sc03430b

short ultrathin CeO_2 nanowires inserted highly porous Co_3O_4 frameworks with different Ce/Co molar ratios, namely, the CeO_2–Co_3O_4 hybrid nanocomposite. This strategy involves the following two separate steps: the facile synthesis of CeO_2 nanowires inserted into ZIF-67 hetero-precursors; and subsequent thermolysis treatment. Besides, the synthetic strategy can be extended to prepare other complex CeO_2 nanowires inserted into $ZnCo_2O_4$ and $NiCo_2O_4$ hybrid nanocomposites. Such unique hybrids take into account the components, hybrid nanostructures and the unique morphologies of the building blocks. More importantly, the as-obtained mixed metal oxides have shown superior performance when evaluated as catalysts in the chemical reduction of NO by CO.

Experimental

Synthesis of ultra-thin CeO_2 nanowires

The synthetic process is accordance with the report by Yu's group. Typically, 2 mmol $Ce(Ac)_3$ is dissolved in a water/ethanol mixture (1/1) and heated in an oil bath. Until the temperature reached 140 °C, 20 mL ammonia is added very fast to the reaction solution. 12 hours later, the products are purified by centrifugation and washed three times with water and dried at room temperature overnight.

Synthesis of CeO_2–ZIF-67 precursors

20 mg of the as-obtained CeO_2 nanowires are dispersed in 20 mL absolute methanol. Under vigorous stirring, 4 mmol 2-methylimidazole powder is added. 30 min later, 5 mL of a $Co(NO_3)_2$ methanol solution (0.2 M) is injected into the mixture. The reaction only needs one hour. Finally, the products are purified by centrifugation and washed with methanol and dried for further application.

Synthesis of CeO_2–ZIF-67 (Ni, Co or Zn, Co)

The synthetic strategy is very similar to CeO_2–ZIF-67. The only difference is using Ni, Co (or Zn, Co) mixed metal ions to replace the Co ions.

Synthesis of CeO_2–Co_3O_4 nanoframeworks

The dried precursors are further annealed at 400 °C for 60 min at a heating rate of 1 °C min^{-1}.

Characterization

The X-ray diffraction patterns of the products were collected on a Rigaku-D/max 2500 V X-ray diffractometer using Cu-K_α radiation (λ = 1.5418 Å), with an operation voltage and current maintained at 40 kV and 40 mA. Transmission electron microscopy (TEM) images were obtained with a TECNAI G2 high-resolution transmission electron microscope operating at 200 kV. The catalytic performances of the catalysts were monitored on-line by a mass spectrogram.

Catalytic test: NO reduction

50 mg of catalyst was put in a stainless steel reaction tube. The experiment was carried out under a flow of reactant gas mixture (2000 ppm CO, 2000 ppm CO, balance Ar) at a rate of 50 mL min^{-1}.

Results and discussion

The whole synthetic process is schematically illustrated in Fig. 1. First of all, the ultrathin CeO_2 nanowires are obtained *via* the previously reported method (as shown in the Experimental part; the corresponding TEM images are shown in Fig. 2A). Subsequently, a certain amount of CeO_2 nanowires was dispersed in methanol by ultrasound treatment followed by the addition of 2-methylimidazole to the mixture and stirring for 30 min. The preliminary mixing of CeO_2 nanowires and 2-methylimidazole together is necessary. This is because the 2-methylimidazole ligand can coordinate with Ce ions on the surface, which is a prerequisite for the successful surface growth of ZIF-67 nanocrystals.

The structure of the as-formed inserted hybrid nanostructures was characterized by powder X-ray diffraction (XRD), transition electron microscopy (TEM), energy-dispersive X-ray spectroscopy (EDX), high-angle annular dark-field scanning transmission electron microscopy (HAADF-STEM) and thermogravimetric analysis (TGA). The XRD pattern of the CeO_2–ZIF-67 hybrids is shown in Fig. S1.† The diffraction peak of CeO_2 is relatively weak, and it is difficult to distinguish directly the presence of CeO_2. The small particle size and poor crystallization are considered to be the main reasons. Furthermore, the diffraction peaks between 10° to 20° match well with the ZIF-67 crystals.[23] Further investigation by TEM imaging was also conducted and is shown in Fig. 2B and C, indicating that the as-obtained precursors are uniform and monodisperse sub-300 nm polyhedra. Interestingly, the enlarged TEM image in Fig. 2D confirms that the original long nanowires have disappeared and several short and ultra-thin ones are formed and inserted *in situ* into the ZIF-67 nanocrystals. Some of the short nanowires are enclosed completely and some of them are partly embedded in the polyhedra leaving parts of the nanowires exposed outside. Such a self-inserted hybrid nanostructure is easily observed in Fig. 2E. Additionally, the HRTEM image in Fig. 2F illustrates that the lattice spacing of 0.31 nm corresponds well with the characteristic (111) planes of fluorite phase CeO_2. A further STEM image is shown in Fig. 2G, in which the inserted one-dimensional nanostructures are easy to distinguish owing to

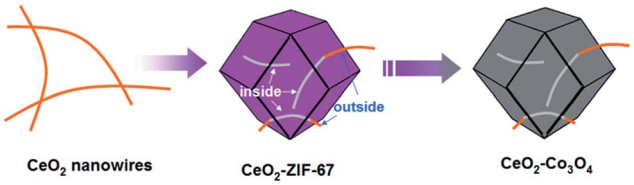

Fig. 1 The synthetic steps of short CeO_2 nanowires inserted porous Co_3O_4 nanoframeworks.

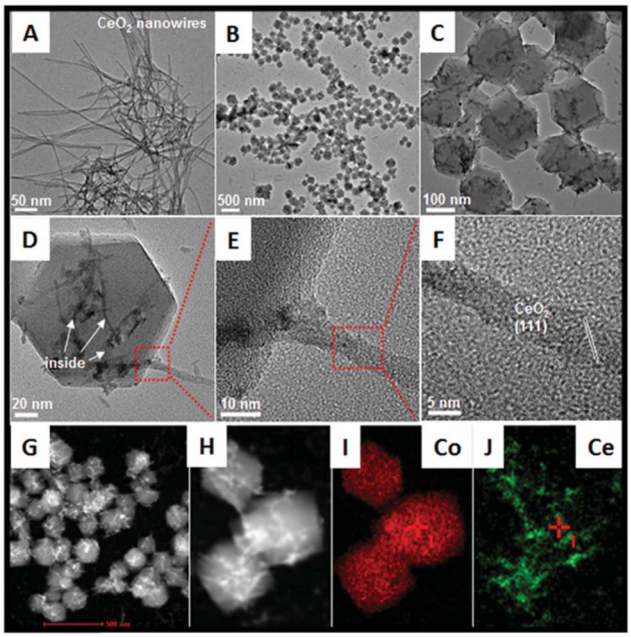

Fig. 2 TEM images of (A) bare CeO_2 nanowires; (B) to (F) ZIF-67 nanocrystals with short CeO2 nanowires inserted; (G) the corresponding STEM image; (H) to (J) STEM-mapping analyses about the as-obtained precursors.

their brighter contrast. HAADF-STEM-mapping image has also been used to analyze further the distribution of Ce and Co elements in the precursors. As shown in Fig. 2H–J, the polyhedra are composed by only Co element; and Ce element exhibits random one-dimensional distribution, both inserted and outside the polyhedra. The formation process of such unique hybrids is supposed to occur by the pre-mixing of CeO_2 and 2-methylimidazole molecules making parts of the 2-methylimidazole molecules coordinate with Ce ions on the surface of CeO_2 nanowires. The addition of Co^{2+} into the reaction solution causes the surface nucleation of ZIF-67 nanocrystals. However, the rigid CeO_2 nanowires are not stable enough, such that during the growth process of ZIF-67 nanocrystals, CeO_2 nanowires are cut into several short pieces.

In addition, the rapid growth rate of ZIF-67 nanocrystals causes the as-formed short CeO_2 nanowires to embed or insert successfully into the ZIF-67 nanocrystals. From these results, some important advantages of the unique hybrid nanostructures should be noted: (1) using MOFs as the precursors greatly simplifies the difficulty in hybridization of CeO_2 and other kinds of transition metal oxides. The surface nucleation and *in situ* self-inserted growth behavior cause the two different components to be strongly coupled together, and more importantly, such a synthesis is a clean strategy, in that the whole process does not use of any additive agent; (2) the organic part can be removed completely without any residue *via* a simple heating treatment; (3) this is the first time to combine one-dimensional CeO_2 and a three-dimensional transition metal oxide (precursor) together, which is considered very interesting for the efficiency of hybridization for the optimization of the catalytic performances.

Furthermore, TG analysis is also conducted in order to determine a suitable annealing temperature. With the data shown in Fig. S2,† an obvious weight-loss peak has appeared at about 400 °C, which matches well with the previous reports.[31] Moreover, simply changing the feeding molar ratio of Ce and Co can cause the component-evolution of the hybrids. With the TEM images shown in Fig. S3,† doubling the molar ratio of Ce/Co leads to the growth of ZIF-67 nanocrystals be much looser (CeO_2–ZIF-67-1). On the opposite, halving the molar ratio of Ce/Co causes more intensive ZIF-67 nanocrystals formed with CeO_2 nanowires inserted (CeO_2–ZIF-67-3). The corresponding inductively coupled plasma atomic emission spectrometry (ICP-AES) of the three samples are also taken and shown in Table S1.† The final mixed metal oxides with different Ce/Co molar ratios are named as CeO_2–ZIF-67-1 (CeO_2–Co_3O_4-1), CeO_2–ZIF-67-2 (CeO_2–Co_3O_4-2) and CeO_2–ZIF-67-3 (CeO_2–Co_3O_4-3).

In addition, such a synthesis strategy can be further extended to the fabrication of one-dimensional CeO_2 inserted mixed metal–organic frameworks (ZIF-67 [Zn, Co] or ZIF-67 [Ni, Co]). As shown in Fig. 3, the as-obtained precursors have similar morphologies to CeO_2–ZIF-67 (Co). The smooth surface of the MOFs and the inserted hybrid nanostructure are easy to distinguish. Further HAADF-STEM-mapping analyses have also confirmed the as-obtained hybrids are composed of Ce, Zn (Ni) and Co elements, that the polyhedra is composed by Ni and Co

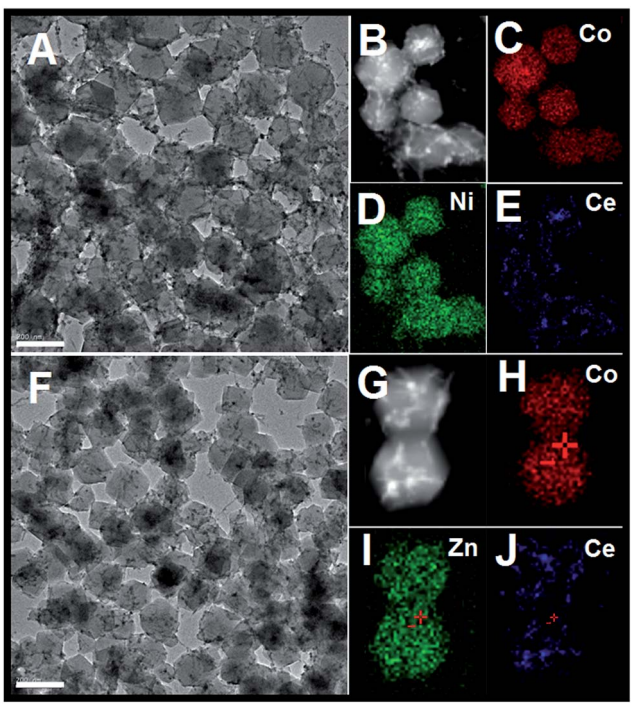

Fig. 3 (A) TEM image of CeO_2 inserted ZIF-67 (Ni, Co) precursors; (B to E) the corresponding STEM-mapping analyses; TEM image of CeO_2 inserted ZIF-67 (Zn, Co) precursors; (G to J) the corresponding STEM-mapping analysis; the scale bar in (A and F) is 200 nm.

(or Zn and Co) elements, and the Ce elements are in the form of one-dimensional nanostructures.

Subsequently, the precursors are annealed at 400 °C for 60 min to accomplish the oxidation process. The XRD data is shown in Fig. 4E. Compared with the data of CeO_2–ZIF-67 precursors, the weak diffraction peaks of ZIF-67 are totally absent in the XRD pattern and the (220), (311), (400) and (440) peaks are unambiguously ascribed to a typical Co_3O_4 nanostructure. Importantly, a small diffraction peak at 28.7° is observed clearly, which can be attributed to the (111) planes of CeO_2. TEM observations have been used to obtain further insight into the structural information of annealed samples. As shown in Fig. 4A, the products maintain well the structural morphology of CeO_2–ZIF-67 even after the high-temperature annealing process, but the particle sizes are decreased significantly to about 200 nm. The increased surface roughness and the tiny holes on the surface of CeO_2–Co_3O_4 can be ascribed to the liberation of CO_2 and H_2O during the heating treatment. CeO_2 components kept their original one-dimensional nanostructures, which could be easily distinguished by their different contrast and growth-orientation as marked by the red arrows in Fig. 4A. More interestingly, parts of the un-embedded CeO_2 could be also found outside the Co_3O_4 porous nanostructures with the data shown in Fig. 4B. The HRTEM images in Fig. 4C and D illustrate that the lattice spacing of 0.31 nm and 0.23 nm corresponds well with the characteristic (111) planes of the fluorite phase of CeO_2 and the (220) planes of Co_3O_4, respectively. The X-ray photoelectron spectroscopy (XPS) curves (Fig. S4†) show that the two peaks at 780 eV and 791 eV correspond well to the Co $2p_{5/2}$ and $2p_{3/2}$ spin orbit peaks, respectively, while the peaks at 881.9 eV and 900.2 eV can be assigned to Ce $3d_{5/2}$ and $3d_{3/2}$ spin orbit peaks, respectively. The specific surface area of the as-obtained CeO_2–Co_3O_4-2 sample calculated from the BET curve (Fig. S5†) reaches about 64.76 m^2 g^{-1}. In addition, the IR spectra of the 2-methylimidazole molecule and the final CeO_2–Co_3O_4-2 sample are also investigated and shown in Fig. S6.† No observed peaks could be found in the final products, indicating that no functional groups were left after the heating treatment.

The catalytic reaction: CO + NO → CO_2 + N_2 has received increased attention, this is because the reaction realizes the goal of reduction of NO and oxidation of CO at the same time. However, compared with the traditional model reaction, CO oxidation, the above catalytic reaction, reduction of NO by CO, is much harder to accomplish. This requires the catalyst to have higher activity, stability and selectivity. The evaluation of catalytic activity was performed in a fixed-bed reactor coupled online with a mass spectrometer. Fig. 5A shows the typical conversion ratio of NO to N_2 as a function of reaction temperature over the five catalysts with different molar ratios of Ce/Co with a feed gas containing 2000 ppm CO. 2000 ppm NO (balanced with Ar) was allowed to pass through the reactor at a gas hourly space velocity (GHSV) of 120 000 mL (g^{-1} h^{-1}). As illustrated in Fig. 5, it seems obvious that the pure CeO_2 nanowires only exhibit limited catalytic activity. Even when increasing the reaction temperature to about 300 °C, the conversion is still almost 0%. A porous Co_3O_4 nanoframework exhibits a much higher catalytic performance. At 200 °C, over 50% NO is converted. Interestingly, all of the three kinds of hybrid nanostructure are more active than pure CeO_2 or Co_3O_4. CeO_2–Co_3O_4-2 has the highest catalytic properties. The conversion reaches 38.7%, 93.8% and 96.9 at 150 °C, 200 °C and 250 °C, respectively.

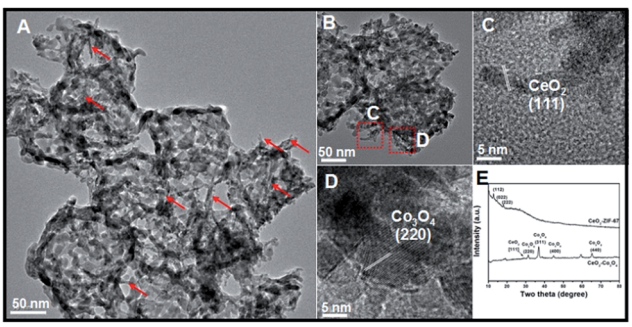

Fig. 4 (A and B) TEM images of CeO_2–Co_3O_4 hybrid nanoframeworks; (C and D) the corresponding HRTEM images; (E) XRD spectra of CeO_2–ZIF-67 precursors and CeO_2–Co_3O_4 products.

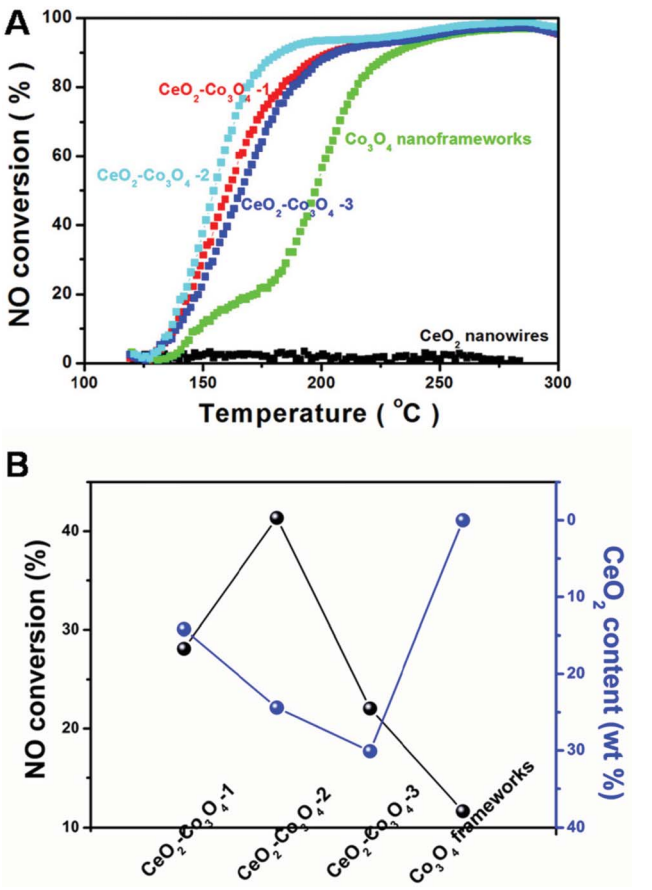

Fig. 5 (A) NO conversion curves of CeO_2 nanowires, CeO_2–Co_3O_4-1, CeO_2–Co_3O_4-2, CeO_2–Co_3O_4-3 and Co_3O_4 nanoframeworks; (B) the relationship between NO conversion and CeO_2 content in the five as-obtained catalysts.

For comparison, increasing or decreasing the Ce/Co ratio causes activity loss. At the reaction temperature of 150 °C (or 200 °C), CeO_2–Co_3O_4-1 and CeO_2–Co_3O_4-3 can only convert 30.7% (or 88.8%) and 23.8% (or 87.7%) of NO, respectively. This is a typical component-dependent catalytic performance. It is well-known that the CeO_2 dispersion and the interaction between cobalt oxide and ceria play an important roles in determining the catalytic activity. Therefore, a certain proportion of CeO_2 in Co_3O_4 is the most suitable to exhibit the best catalytic activity. A similar phenomenon usually happens in other kinds of CeO_2-based mixed metal oxides as catalysts in heterogeneous catalytic reactions.[32–34] In order to display intuitively the relationship between the catalytic activity and the component, Fig. 5B illustrates the component-dependent conversion at 150 °C, indicating that the as-obtained hybrid samples exhibit component-dependent catalytic performances. It should be also noted that limited N_2O could be detected during the whole test catalyzed by the hybrid component, illustrating the unique catalytic selectivity. Further aging tests have also been taken by monitoring the NO conversion catalyzed by CeO_2–Co_3O_4-2 sample at 180 °C for 9 continuous hours. As shown in Fig. S7,† the as-obtained CeO_2–Co_3O_4-2 samples keep their catalytic performance; 83% conversion could also be achieved 9 hours later. This result suggests the high stability of the CeO_2–Co_3O_4 hybrid nanostructure.

In order to clarify the redox relationship and their synergistic effects for improved catalytic performance, we further tested the H_2-TPR profiles of the five nanocatalysts. As shown in Fig. 6, two broad TPR peaks observed at 375 °C and 600 °C for CeO_2 can be attributed to the reduction of the surface capping oxygen and the bulk oxygen of ceria, respectively.[12,35] For pure Co_3O_4 nanoframeworks, the two reduction peaks at about 337 °C and 497 °C match well with the previous reports by Venezia's group.[36] For comparison, the mixed metal oxides show relatively high reducibility with respect to pure CeO_2 and Co_3O_4 due to the significant interaction between the two phases. Moreover, a noticeable new reduction peak below 250 °C appears in all three hybrids. With the increase of Co_3O_4 content in the mixed metal oxide, such new reduction peaks become stronger and stronger, indicating that the synergistic effect is continuously enhanced. Comparing CeO_2–Co_3O_4-2 with CeO_2–Co_3O_4-3, although the peak position and intensity of the new peak are similar, the obvious blue-shifts of the following two peaks have been observed very clearly. Combined with the above analyses, H_2-TPR profiles confirmed firmly that the CeO_2–Co_3O_4-2 sample has the highest activity, which is in accordance with the catalytic results.

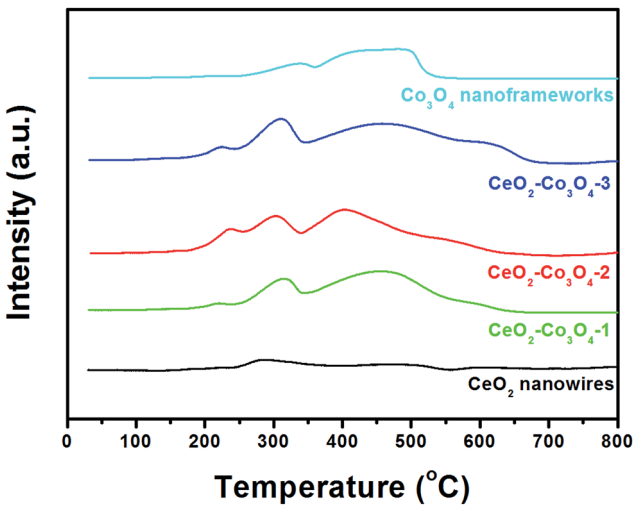

Fig. 6 H_2-TPR profiles of CeO_2 nanowires, CeO_2–Co_3O_4-1, CeO_2–Co_3O_4-2, CeO_2–Co_3O_4-3, Co_3O_4 nanoframeworks.

By referring to the Eley–Rideal mechanism and the Langmuir–Hinshelwood mechanism,[37–40] the possible advantages of such a hybrid nanostructure in the reduction of NO by CO have been supposed as:

(1) Co_3O_4 can react with CeO_2 to form CoO during the catalytic reaction. In other words, the interaction between Co_3O_4 and CeO_2 can greatly increase the stability of CoO and elongate the Co–O bond on the CeO_2–Co_3O_4 interface.[37]

(2) CeO_2 has a high oxygen storage capacity and well-known redox properties (couples of Ce^{4+}/Ce^{3+}), which produce lots of active oxygen available for the oxidation process. The presence of mobile oxygen and weak Co–O bonds in cobalt oxide were reflected in the relatively low ΔH for O_2 vaporization.[40]

(3) Such a self-inserted hybrid nanostructure gives the final products a large specific surface area and a strongly coupled interface.

Conclusions

In conclusion, a novel low-cost and facile synthesis strategy has been successfully developed to create unique hybrid nanostructures composed by one-dimensional CeO_2 nanostructures inserted into porous Co_3O_4 frameworks. The synthesis strategy involves the *in situ* formation of CeO_2 nanowires self-inserted into ZIF-67 precursors and subsequent thermal annealing in air. During the annealing process, porous cages are formed and several short CeO_2 nanowires have been inserted into the three-dimensional Co_3O_4 nanocages. Such a synthesis strategy could be extended to the synthesis of CeO_2 inserted into $NiCo_2O_4$ and $ZnCo_2O_4$ hybrid nanocomposites. When evaluated as heterocatalysts for the NO reduction by CO, they exhibited component-dependent catalytic properties. The CeO_2–Co_3O_4-2 has shown the highest catalytic performance, much better than even the current reported Ce–Cu mixed metal oxide, which is also synthesized *via* a MOFs-assistant method.[3] This is the first time that the goal of optimization of the catalytic performance of CeO_2-based mixed metal oxides has been realized by taking account of the components of the hybrid nanostructure as well as the size and shape of each component. It is believed that the developed synthesis and the obtained unique hybrid nanostructures have opened a new window to design new kinds of "noble metal free" nanocatalysts.

Acknowledgements

The authors are grateful for financial aid from the National Natural Science Foundation of China (Grant No. 21221061,

51372242, 91122030, 21401186 and 21210001), the Hong Kong, Macao and Taiwan Science and Technology Cooperation Special Project of Ministry of Science and Technology of China (No. 2014DFT10310), the Program of Science and Technology Development Plan of Jilin Province of China (No. 20140201007GX), the National Key Basic Research Program of China (No. 2014CB643802) and the Jilin Province Youth Foundation (20130522122JH).

Notes and references

1 Y. Liang, H. Wang, P. Diao, W. Chang, G. Hong, Y. Li, M. Gong, L. Xie, J. Zhou, J. Wang, T. Z. Regier, F. Wei and H. Dai, *J. Am. Chem. Soc.*, 2012, **134**, 15849.
2 S. Y. Song, X. Wang and H. J. Zhang, *NPG Asia Mater.*, 2015, **7**, e179.
3 S. Li, N. Wang, Y. Yue, G. Wang, Z. Zu and Y. Zhang, *Chem. Sci.*, 2015, **6**, 2495.
4 Y. Wang, Y. Shao, D. Matson, J. Li and Y. Lin, *ACS Nano*, 2010, **4**, 1790.
5 J. Wang, H. Zhong, Y. Qian and X. Zhang, *Angew. Chem., Int. Ed.*, 2013, **52**, 5248.
6 H. Zhong, J. Wang, Y. Zhang, W. Xu, W. Xing, D. Xu, Y. Zhang and X. Zhang, *Angew. Chem., Int. Ed.*, 2014, **53**, 14235.
7 X. Wang, D. P. Liu, S. Y. Song and H. J. Zhang, *J. Am. Chem. Soc.*, 2013, **135**, 15864.
8 X. Y. Li, X. Wang, D. P. Liu, S. Y. Song and H. J. Zhang, *Chem. Commun.*, 2014, **50**, 7198.
9 W. Liu, X. Liu, L. Feng, J. Guo, A. Xie, S. Wang, J. Zhang and Y. Yang, *Nanoscale*, 2014, **6**, 10693.
10 A. Jia, S. Jiang, J. Lu and M. Luo, *J. Phys. Chem. C*, 2010, **114**, 21605.
11 H. Yen, Y. Seo, S. Kaliaguine and F. Kleitz, *Angew. Chem., Int. Ed.*, 2012, **51**, 12032.
12 X. Wang, D. Liu, J. Li, J. Zhen and H. Zhang, *NPG Asia Mater.*, 2015, **7**, e158.
13 H. Bao, Z. Zhang, Q. Hua and W. Huang, *Langmuir*, 2014, **30**, 6427.
14 J. Zhen, X. Wang, D. Liu, Z. Wang, J. Li, F. Wan, Y. Wang and H. Zhang, *Nano Res.*, 2015, **8**, 1944.
15 J. Zhen, X. Wang, D. Liu, S. Song, Z. Wang, Y. Wang, J. Li, F. Wang and H. Zhang, *Chem.–Eur. J.*, 2014, **20**, 4469.
16 Q. Xie, Y. Zhao, H. Guo, A. Lu, X. Zhang, L. Wang, M. Chen and D. Peng, *ACS Appl. Mater. Interfaces*, 2014, **6**, 421.
17 F. Wang, X. Wang, D. Liu, J. Zhen, J. Li, Y. Wang and H. Zhang, *ACS Appl. Mater. Interfaces*, 2014, **6**, 22216.
18 Y. Liu, X. Sun, Z. Zhou and Y. Lei, *J. Mater. Chem. A*, 2014, **2**, 14038.
19 D. D. Zhang, S. W. Eaton, Y. Yu, L. Dou and P. D. Yang, *J. Am. Chem. Soc.*, 2015, **137**, 9230.
20 R. Wu, J. F. Zhang, Y. M. Shi, D. L. Liu and B. Zhang, *J. Am. Chem. Soc.*, 2015, **137**, 6983.
21 L. Zhang, H. B. Wu and X. W. Lou, *J. Am. Chem. Soc.*, 2013, **135**, 10664.
22 S. Y. Song, X. Wang, S. L. Li, Z. Wang, Q. Zhu and H. J. Zhang, *Chem. Sci.*, 2015, **6**, 6420.
23 H. Hu, B. Y. Guan, B. Y. Xia and X. W. Lou, *J. Am. Chem. Soc.*, 2015, **137**, 5590.
24 X. Z. Song, S. Y. Song, S. N. Zhao, Z. M. Hao, M. Zhu, X. Meng, L. L. Wu and H. J. Zhang, *Adv. Funct. Mater.*, 2014, **24**, 4034.
25 M. Zhu, X. Z. Song, S. Y. Song, S. N. Zhao, X. Meng, L. L. Wu, C. Wang and H. J. Zhang, *Adv. Sci.*, 2015, **2**, 1500012.
26 H. X. Zhong, J. Wang, Y. W. Zhang, W. L. Xu, W. Xing, D. Xu, Y. F. Zhang and X. B. Zhang, *Angew. Chem., Int. Ed.*, 2014, **53**, 14235.
27 J. Wang, H. X. Zhong, Y. L. Qin and X. B. Zhang, *Angew. Chem., Int. Ed.*, 2013, **52**, 5248.
28 W. Zhang, Z. Y. Wu, H. L. Jiang and S. H. Yu, *J. Am. Chem. Soc.*, 2014, **136**, 14385.
29 J. Tang, R. R. Salunkhe, J. Liu, N. L. Torad, M. Imura, S. Furukawa and Y. Yamauchi, *J. Am. Chem. Soc.*, 2015, **137**, 1572.
30 J. J. Zhou, P. Wang, C. X. Wang, Y. T. Goh, Z. Fang, P. B. Messersmith and H. W. Duan, *ACS Nano*, 2015, **9**, 6951.
31 G. Huang, F. F. Zhang, X. C. Du, Y. L. Qin, D. M. Yin and L. M. Wang, *ACS Nano*, 2015, **9**, 1592.
32 Y. Gao, K. Xie, W. Wang, S. Mi, N. Liu, G. Pan and W. Huang, *Catal. Sci. Technol.*, 2015, **5**, 1568.
33 F. Zhao, M. Gong, G. Zhang and J. Li, *J. Rare Earths*, 2015, **33**, 604.
34 S. Hu, F. Zhou, L. Wang and J. Zhang, *Catal. Commun.*, 2011, **12**, 794.
35 Y. Zuo, X. Huang, L. Li and G. Li, *J. Mater. Chem. A*, 2013, **1**, 374.
36 L. F. Liotta, H. Wu, G. Pantaleo and A. M. Venezia, *J. Mater. Chem. A*, 2013, **3**, 2085.
37 J. Luo, M. Meng, X. Li, X. Li, Y. Zha, T. Hu, Y. Xie and J. Zhang, *J. Catal.*, 2008, **254**, 310.
38 V. Shapovalov and H. Metiu, *J. Catal.*, 2007, **245**, 205.
39 G. Sedmak, S. Hocevar and J. Levec, *J. Catal.*, 2003, **213**, 135.
40 Q. Yang, F. Gu, Y. Tang, H. Zhang, Q. Liu, Z. Zhong and F. Su, *RSC Adv.*, 2015, **5**, 26815.